Electron-impact excitation cross sections from the xenon $J=2$ metastable level

R. O. Jung, John B. Boffard, L. W. Anderson, and Chun C. Lin
Department of Physics, University of Wisconsin, Madison, Wisconsin 53706, USA

(Received 11 May 2005; published 25 August 2005)

Cross sections for electron-impact excitation from the $5p^5 6s$ $J=2$ metastable level of xenon to the lowest six levels of the $5p^5 6p$ configuration have been measured. The cross sections generally have very large magnitudes (10^{-15} cm^2) and scale with the corresponding optical oscillator strengths. The substantial variations observed in the energy dependence of the cross sections for the six levels can also be related to the optical oscillator strengths. Cross sections for excitation out of the $J=2$ metastable level into the upper four levels of the $5p^5 6p$ configuration are much smaller. The large disparity in cross sections between the upper and lower groups is explained in terms of the electronic structure of the excited states of xenon.

DOI: 10.1103/PhysRevA.72.022723 PACS number(s): 34.80.Dp, 34.80.My, 52.20.Fs

I. INTRODUCTION

Weakly ionized xenon plasmas are used in a number of current applications, including mercury-free fluorescent lighting [1–4] and flat-panel plasma displays [5]. In these applications, the vacuum ultraviolet (VUV) emissions from the decay of the two $J=1$ $5p^5 6s$ resonance levels are used to excite phosphors to produce a white-light output. Electron-impact excitation into the two metastable levels of the $5p^5 6s$ configuration lowers the efficiency of these devices, unless the population of atoms in these metastable levels are transferred to the resonance levels before the atoms are lost to wall collisions. One way of coupling the metastable levels to the resonance levels is via electron-impact excitation either directly from the metastable levels to the resonance levels or by excitation into higher levels followed by radiative decay to the resonance levels [2]. In this work we report cross sections for electron-impact excitation from the Xe $5p^5 6s$ $J=2$ metastable level into the lowest six levels of the $5p^5 6p$ configuration.

In addition to providing a mechanism for transferring the metastable levels into the resonance levels, the optical emissions arising from electron-impact excitation of rare-gas atoms (including Xe) have important applications in the field of optical plasma diagnostics [6,7]. In trace-rare-gas optical emission spectroscopy (TRG-OES) developed by Donnelly and his coworkers, a small mixture of rare-gas atoms (1% each of He, Ne, Ar, Kr, and Xe) is added to a plasma and the emissions in the 300–950 nm wavelength range are used to determine plasma properties, such as the electron energy distribution function (EEDF) [7]. To determine the EEDF, the emission intensities for a number of spectral lines with a wide range of onset energies are used. Xe has the lowest onset energy for excitation from the ground state, but this still requires electrons with energies in excess of 9.5 eV. To sample the EEDF at even lower energies, one may employ emission lines that are dominated by the contribution from electron-impact excitation of metastable levels, which have much lower energy thresholds (~1.5 eV) [8].

Studies of electron-impact excitation out of the metastable levels of Xe are of great interest also from the standpoint of fundamental collision physics, particularly in relating the excitation cross sections to atomic structure. Within an excited configuration Xe($5p^5 nl$) the energy levels segregate into two tiers separated by ~1.4 eV as shown in Fig. 1. This is due to the relatively large spin-orbit splitting of Xe$^+$($5p^5$) into two levels corresponding to the total core-angular momentum j_c equal to 3/2 and 1/2, designated as $^2P_{3/2}$ and $^2P_{1/2}$. For the first excited configuration $5p^5 6s$ the $^2P_{3/2}$ ion core couples to the $6s$ electron to form $J=2$ and $J=1$ levels, which are called the $1s_5$ and $1s_4$ levels, respectively, in Paschen's notation. Similarly the $^2P_{1/2}$ ion core couples with the $6s$ electron to form two levels with $J=1$ ($1s_2$) and $J=0$ ($1s_3$). The $J=2$ ($1s_5$) and $J=0$ ($1s_3$) levels are metastable. Since the spin-orbit interaction within the ion core is much stronger than the coupling of the outer electron with the ion core, the core-angular momentum j_c is a good quantum number and the four levels of the $5p^5 6s$ configuration segregate into two groups (for $j_c=3/2$ and 1/2), which are separated by 1.4 eV, the spin-orbit splitting of the ion core. Likewise the ten levels of the $5p^5 6p$ configuration exhibit the same two-tier structure with an upper quartet ($j_c=1/2$ with $J=0,1,2,1$ called $2p_1$ through $2p_4$ in Paschen's notation) and a lower sextet ($j_c=3/2$ with $J=0,2,1,3,2,1$ or $2p_5$ through $2p_{10}$). This is to be contrasted with the electronic structure of the lighter rare gases. Both Ar and Ne have much smaller ion-

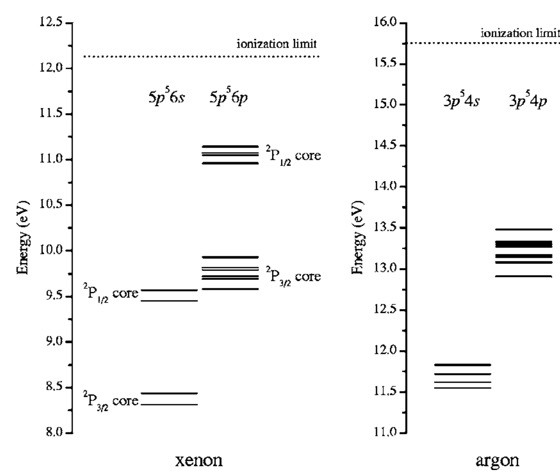

FIG. 1. Comparison of Xe and Ar energy levels.

TABLE I. Xe energy levels in various labeling schemes. For almost all levels the *LS* coupling scheme is not relevant since *LS* basis constituents with the same *J* are mixed together; only levels with a unique *J* value within each configuration can be unambiguously labeled in the *LS* scheme under the one-configuration approximation. *E* is the energy of the level relative to the ground state.

Paschen	J	j_c	Racah	E (eV)	LS
$2p_1$	0	1/2	$6p'[\frac{1}{2}]_0$	11.14	mix
$2p_2$	1	1/2	$6p'[\frac{1}{2}]_1$	11.07	mix
$2p_3$	2	1/2	$6p'[\frac{3}{2}]_2$	11.05	mix
$2p_4$	1	1/2	$6p'[\frac{3}{2}]_1$	10.96	mix
$2p_5$	0	3/2	$6p[\frac{1}{2}]_0$	9.93	mix
$2p_6$	2	3/2	$6p[\frac{3}{2}]_2$	9.82	mix
$2p_7$	1	3/2	$6p[\frac{3}{2}]_1$	9.79	mix
$2p_8$	3	3/2	$6p[\frac{5}{2}]_3$	9.72	$^3D_3$
$2p_9$	2	3/2	$6p[\frac{5}{2}]_2$	9.69	mix
$2p_{10}$	1	3/2	$6p[\frac{1}{2}]_1$	9.58	mix
$1s_2$	1	1/2	$6s'[\frac{1}{2}]^o_1$	9.57	mix
$1s_3$	0	1/2	$6s'[\frac{1}{2}]^o_0$	9.45	$^3P_0$
$1s_4$	1	3/2	$6s[\frac{3}{2}]^o_1$	8.44	mix
$1s_5$	2	3/2	$6s[\frac{3}{2}]^o_2$	8.31	$^3P_2$

core spin-orbit interactions, which are overpowered by the coupling of the ion core with the outer electron. In these cases j_c is no longer a good quantum number, so no two-tier structure is seen in the Ar($3p^54s$) and Ar($3p^54p$) configurations included in Fig. 1.

In addition to the Paschen notation used in this paper, the energy levels of xenon are also widely labeled using Racah notation, which more clearly indicates the ion core of the level. In this scheme a $5p^5nl$ level is labeled $nl[K]_J$. A prime on the nl indicates a level has $j_c=1/2$, whereas levels with $j_c=3/2$ are left unprimed. K is the intermediate vector sum of j_c and l, the orbital angular momentum of the valence electron. The total angular momentum J is the vector sum of K, and the spin $s=1/2$ of the valence electron. This particular order of angular momentum coupling would lead to a number of closely spaced doublets for each value of K. Since this is not always the case, the K values in this notation are best viewed as labels rather than being physically realistic definitions. Table I is provided to aid in switching between the Racah and Paschen labeling schemes.

The two-tier structure of the Xe energy levels has a profound influence on the excitation cross sections. Excitation out of a metastable level of the Xe($5p^56s$) configuration into one of the Xe($5p^56p$) levels may or may not involve a change in the core quantum number j_c. The core-preserving excitations are expected to be more favorable than the core-changing excitations since in the latter case a single collision would have to both excite the outer electron and change the core. This core propensity has been reported recently in a study of electron-impact excitation out of the metastable levels of Kr into the ten Kr($4p^55p$) levels, where the core-preserving excitations dominate the core-changing ones [9]. In this work we report excitation cross sections out of the $1s_5$ metastable level of Xe and discuss the results in light of the core effect and in comparison to the corresponding results of Ar in which the ion core plays a much less significant role.

II. EXPERIMENT

A. Apparatus

Two sources of metastable Xe atoms were used in this work: a hollow cathode discharge for low-energy relative measurements and a charge-exchange fast beam source for high-energy absolute measurements. Detailed descriptions of both sources have been given previously [10,11], therefore we only present a brief overview of each source.

The first source of Xe* atoms consists of a hollow cathode discharge. Metastable xenon atoms are created inside the discharge (400 V, 50 mA) and exit through a 1 mm hole in the base of the cathode. An 85% He–15% Xe mixture was used as the feed gas (total pressure of 4.5 Torr). The helium gas is necessary to (i) create a stable discharge containing a high number density of xenon metastable atoms and (ii) reduce the sputtering damage to the hollow cathode relative to that of a pure xenon discharge. The xenon metastable atoms that exit the discharge are excited with a variable energy monoenergetic electron beam. Fluorescence from the decay of excited atoms is collected by a lens, passed through a narrow-band interference filter (0.5–1.2 nm FWHM) for spectral isolation, and detected by a photomultiplier tube (PMT) operating in photon-counting mode. Two different PMTs were used in this work: for wavelengths <900 nm, an EMI 9658B (S-20 cathode) PMT was used, and for wavelengths >900 nm, a Hamamatsu R5509-72 NIR-PMT was used. The axis of the optical system is oriented at an angle of 60 deg with respect to the electron-beam axis. This angle is very close to the "magic angle" of 54.7 deg, where the emission intensity is equal to the average intensity independent of the polarization of the radiation [12]. This does not completely eliminate the possible influence of polarization on our measurements since the light emitted at the magic angle may still be polarized; however, our detection system combination of an interference filter and PMT should be polarization insensitive. Hence, although we make no correction for the polarization of the fluorescence, this should introduce only a negligibly small error in our cross-section measurements.

Above the threshold for ground-state excitation ($\sim$9.5 eV), the excitation signal is dominated by excitation of the overwhelming number of ground-state xenon atoms emerging from the discharge ($n_{gs}/n_{meta}\approx 10^5$). For electron energies below 9 eV, only atoms in levels of the $5p^56s$ configuration contribute to the excitation signal. The fractions of target atoms in the four $5p^56s$ levels were measured via laser-induced fluorescence (LIF) with a single-mode Ti:Sapphire laser pumped by an 8 W argon-ion laser. Essentially, all of the excited atoms in the target were in the $1s_5$ metastable level. No atoms were found in the $1s_2$ and $1s_4$ resonance levels. The number of atoms in the $1s_3$ level depends on the running conditions in the hollow cathode. For the measurements reported here, the ratio of $1s_5$ to $1s_3$ metastable atoms in the target was greater than 200 to 1. This small number of atoms in the $1s_3$ metastable level contributes negligibly to the total signal (see Sec. III). Since the target consists of 85% He gas, helium emissions at transition wavelengths within the bandpass of some of the observed xenon transitions could conceivably also contribute to the excitation signal. Excitation from the ground state of He, however, requires electron energies over 20 eV, which is above the energy range used with this source. Metastable He atoms have a much lower threshold, but were not detected in the target since any present in the discharge are rapidly lost in Penning ionization collisions with Xe.

The second apparatus formed a metastable xenon beam via near-resonant charge-exchange. An rf ion source produces a 3.0 keV xenon ion beam that is passed through a recirculating cesium vapor target. This process preferentially produces Xe atoms in the levels of the $5p^5 6s$ configuration. After the decay of atoms in the $J=1$ resonance levels, the neutral beam consists of $\sim$50% ground-state atoms and 50% metastable atoms (see Sec. II B). The remaining ions in the fast-beam target are removed with a set of deflection plates, and the fast neutral beam is crossed at right angles with a monoenergetic electron beam. As in the hollow cathode experiment, fluorescence from the decay of excited atoms is collected by a lens, passed through a narrow-band interference filter, and detected by a Burle C31034-A02 (GaAs) PMT. The neutral beam flux is measured with a thermal neutral detector, which is calibrated to the easily measured current of the undeflected xenon ion beam. Because of the much higher metastable-to-ground-state fraction in the fast-beam target over that in the hollow cathode source, cross-section measurements could be taken for electron energies well over the threshold for ground-state excitation. The lower target density, however, limited measurements to the levels with the largest cross sections.

B. Data analysis

Absolute cross-section results were obtained in two steps: (i) the cross section for the $1s_5 \rightarrow 2p_8$ cross section was measured in terms of the ground-state$\rightarrow 2p_8$ excitation cross section at high energies using the fast-beam target and (ii) the other five $2p$ levels were measured relative to the $2p_8$ cross section at low energies using the hollow cathode discharge source.

1. $1s_5 \rightarrow 2p_8$ *cross section*

The ratio of the cross sections for excitation into the $2p_8$ ($5p^5 6p\ ^3D_3$) level from the $1s_5$ metastable level to that from the ground state of xenon excitation cross section was measured at 75 eV. The photon counting signal S_m from excitation of the metastable fast-beam target is equal to

$$S_m = \xi(\lambda) Q_m (I_e/e) n_m L_m \Phi_m, \tag{1}$$

where $\xi(\lambda)$ is the total efficiency of the optical system at the 881.9 nm wavelength of the $2p_8 \rightarrow 1s_5$ transition (including solid angle of detection optics, filter transmission, etc.), Q_m is the desired excitation cross section from the $1s_5$ metastable level, I_e is the electron beam current, e is the elementary charge, n_m is the metastable target density, L_m is the effective path length of the electron beam through the metastable beam collected by the optics, and Φ_m is a correction factor to the optical system's detection efficiency, which accounts for the motion of the excited atoms created in the fast-beam target that move out of the optical viewing region. This latter factor can be calculated from the lifetime of the excited level, the velocity of the atoms in the beam, and the sizes of the electron beam and optical viewing region [13]. The metastable target density depends on four factors, the total particle current of the neutral beam, the fraction of $1s_5$ metastable atoms in the beam, the spatial distribution of the beam, and the velocity of atoms in the beam (set by the ion beam energy). To determine the spatial distribution of the metastable Xe beam and the electron beam (required to calculate L_m), a rotating wire is used to measure the profiles of the beams [11]. The total particle current of the neutral beam is measured using a neutral detector that can be run in either secondary electron emission current mode or in a thermal detection mode. Typically, the secondary electron emission current produced by the 3.0 keV xenon beam striking an Al surface is used. The secondary electron emission coefficient of the surface, which depends on the surface conditions, is calibrated by comparing the thermal response of the neutral beam to a known ion beam current.

The fraction of $1s_5$ metastable atoms in the beam is estimated from alkali-noble gas charge-exchange cross sections. The four energy levels of the $5p^5 6s$ configuration of xenon are all near resonant with the ground state of Cs. In the simplest analysis, where each level is populated only according to its statistical weight, charge exchange between Xe^+ and Cs would yield a $1s_5$ fraction in the fast beam of 0.42. A more detailed analysis finds that charge exchange between Xe^+ and Cs preferentially favors the production of the $1s_5$ metastable level [14]. In the reaction

$$Xe^+(5p^5) + Cs \rightarrow Xe(5p^5 6s) + Cs^+ + \Delta E, \tag{2}$$

the energy defects ΔE are small for charge transfer from the $Xe^+(^2P_{1/2})$ level into the $1s_2$ and $1s_3$ levels and from the $Xe^+(^2P_{3/2})$ level into the $1s_4$ and $1s_5$ levels. Since smaller energy defects correspond to larger charge-exchange cross sections, a more complete analysis finds that the final $1s_5$ fraction in the beam depends on the individual energy defects and the composition of the xenon ion beam. These latter effects tend to favor charge exchange into the $1s_5$ metastable level. The $1s_5$ fraction of our fast neutral beam, which also includes a small contribution from resonant production of fast ground-state Xe atoms with background gas, is estimated to be 0.53 ± 0.08.

The final unknown in Eq. (1) that must be eliminated is the efficiency of the optical system $\xi(\lambda)$. This is done by turning off the fast-beam target and filling the collision chamber with a static target of xenon. For this ground-state target, the signal rate is equal to

$$S_g = \xi(\lambda) Q_g (I_e/e) n_g L_g. \tag{3}$$

Since the gas target is spatially uniform, the length of the electron beam imaged by the optical system L_g is only a function of the optical system. The ground-state target density is found by measuring the pressure ($\sim 1.2 \times 10^{-6}$ Torr) in the chamber using a spinning rotor gauge. The ground-state optical emission cross sections for the xenon $5p^5 6p$ levels are highly pressure dependent due to radiation trapping of higher resonant levels that cascade into the $5p^5 6p$ levels [15]. The $J=3$ $2p_8$ level, however, does not receive any cascade contribution directly from $J=1$ $5p^5 ns$ and $5p^5 nd$ resonant levels. As a result, Fons and Lin found that the apparent cross section for the $2p_8$ level is reasonably pressure independent below 5×10^{-4} Torr, with a value of $(200 \pm 40) \times 10^{-20}$ cm^2 at an electron energy of 75 eV [15].

The total uncertainty (systematic and statistical) in the absolute calibration of the $1s_5 \rightarrow 2p_8$ cross section is estimated to be ±35%. The two largest single sources of uncertainty are the determination of the $1s_5$ fraction of the fast beam and the $2p_8$ ground-state excitation cross section (including the extrapolation to zero pressure). At 75 eV we obtain a $1s_5 \rightarrow 2p_8$ cross section of $(13 \pm 4) \times 10^{-16}$ cm^2 and, from the measured energy dependence of the cross section, a value of $(35 \pm 12) \times 10^{-16}$ cm^2 at 6 eV.

2. Remaining $5p^5 6p$ levels

Since the number density of the fast-beam target ($\sim 10^6$ cm^{-3}) is much less than the target density of the hollow cathode discharge source ($\sim 10^{13}$ cm^{-3}), results for the remaining levels were generally only obtained with the hollow cathode source. For these levels the cross section was found by ratioing the signal rates for excitation into the desired $2p_x$ level to the signal rate for the $2p_8$ level at 6.5 eV. This ratioing step eliminates many factors (including the metastable number density, solid angle of the optics, overlap of the electron beam and metastable target, etc.), but does not correct for the optical efficiencies at the two wavelengths observed. In our earlier work on excitation of metastable Ne [16] and Ar [17], we used the previously measured excitation cross sections from the ground-state to eliminate this unknown factor. The extreme pressure dependence of the Xe ground-state excitation cross sections coupled with the high gas pressure in the collision region, however, prevent us from using this technique for Xe. Instead, we measured the desired transition signal from a Xe capillary-tube discharge lamp $S_{\mathrm{lamp}}^{2p_x}$ for which the relative photon flux for each wavelength $D_{\mathrm{lamp}}^{2p_x}$ was previously measured using a monochromator and a calibrated source of spectral irradiance. Combined with the branching fractions $\Gamma_\lambda^{2p_x}$, this yields cross sections from the equation

$$Q_m^{2p_x} = \frac{S_m^{2p_x}}{S_m^{2p_8}} \frac{\Gamma_\lambda^{2p_8}}{\Gamma_\lambda^{2p_x}} \frac{S_{\mathrm{lamp}}^{2p_8}}{S_{\mathrm{lamp}}^{2p_x}} \frac{D_{\mathrm{lamp}}^{2p_x}}{D_{\mathrm{lamp}}^{2p_8}} Q_m^{2p_8}, \tag{4}$$

where $\Gamma_\lambda^{2p_8}=1$, since the 881.9 nm wavelength transition is the only decay channel for this level. To obtain the branching fractions of the remaining levels we use the measurements of Horiguchi *et al.* [18], which agree to within 5% of three other sources: (i) the theoretical values of Aymar and Columbe [19], (ii) the optical emission cross section measurements of Ref. [15], and (iii) the discharge lamp emissions measured for use in Eq. (4). Table II lists the transitions observed in this work along with the branching fractions used.

TABLE II. Xe transitions observed in this work.

Level	Wavelength (nm)	Branching fraction[a]
$2p_5$	828.0	0.998
$2p_6$	823.1	0.700
$2p_7$	916.1	0.915
$2p_8$	881.9	1.000
$2p_9$	904.5	0.363
$2p_{10}$	979.9	0.917

[a]Reference 18.

III. RESULTS

Figures 2–5 display the variation of the apparent cross-sections as a function of incident electron energy for the six levels measured in this work. Cross-section values at selected energies are listed in Table III. The measured apparent cross sections are the sum of the direct excitation cross section and the cascade contribution from excitation into higher levels followed by radiative decays into the level of interest. Since the lifetimes of the $2p_6$ and $2p_8$ levels are generally much shorter than the lifetimes of cascading levels, cross-section measurements made with the fast-beam apparatus have reduced levels of cascade contribution since the long-lived cascade levels decay downstream of where the $2p_x$ emissions are observed [20]. The spatial distribution of the excited-state fluorescence along the direction of motion of atoms in the fast-beam target has also been used to estimate

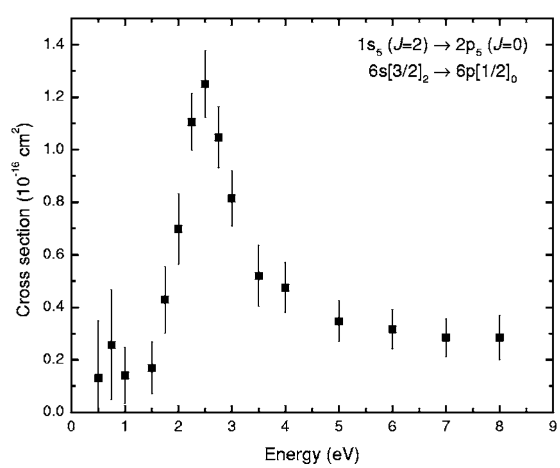

FIG. 2. Excitation function for $J=0$ $2p_5$ level. Error bars are statistical only and do not include the absolute calibration uncertainty of ±35%.

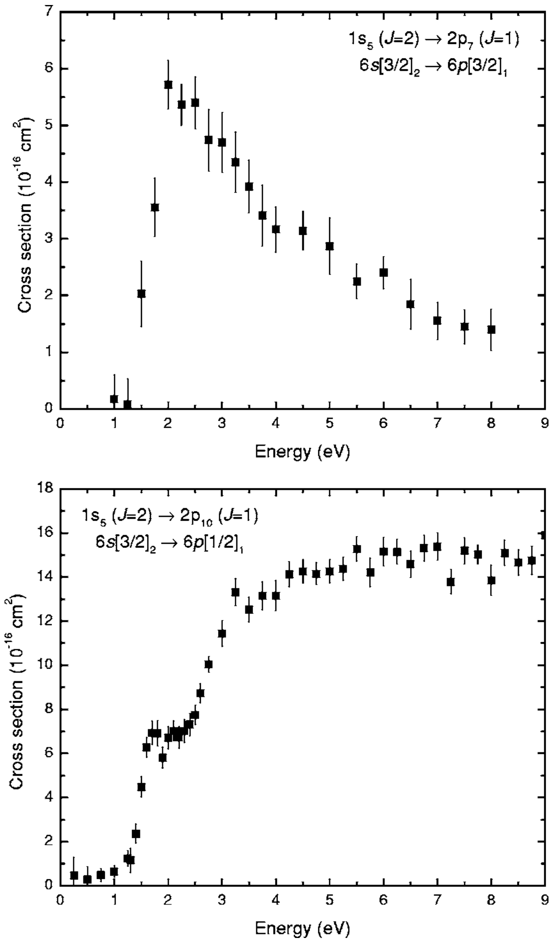

FIG. 3. Excitation functions for $J=1$ $2p_7$ and $2p_{10}$ levels. Error bars are statistical only and do not include the absolute calibration uncertainty of ±35%.

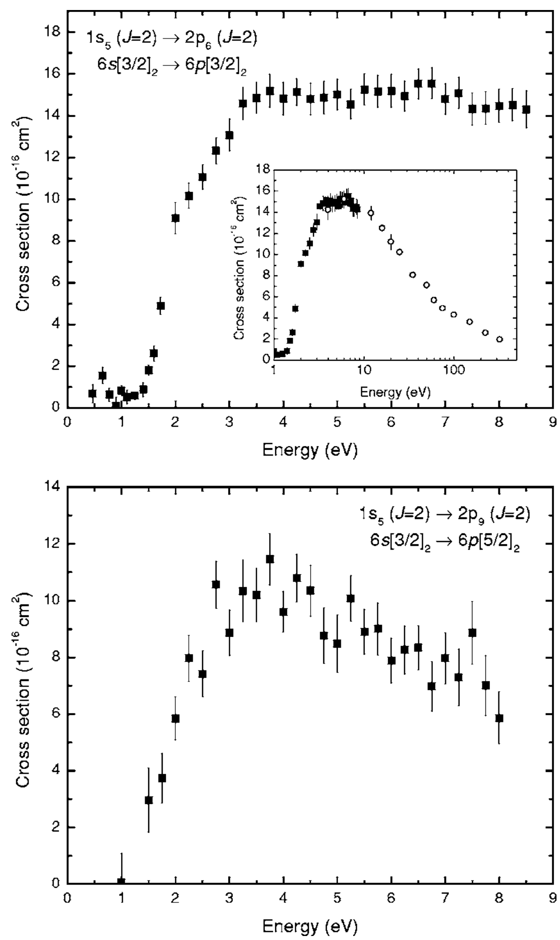

FIG. 4. Excitation functions for $J=2$ $2p_6$ level and $2p_9$ levels. Error bars are statistical only and do not include the absolute calibration uncertainty of ±35%. The insert for the $2p_6$ level includes low-energy data from the hollow cathode source (squares) and high-energy data from the charge exchange source (circles).

the size of the cascade cross sections for excitation of Ne* and Ar*. Unfortunately, the low signal rates obtained with the Xe* (due to the poor PMT sensitivity at long emission wavelengths) combined with the low velocity of the heavy xenon atoms (which decreases our effective temporal sensitivity) prevent a definitive cascade estimate. Based on our previous measurements for the other heavy rare-gas atoms, however, we estimate the cascade contribution to be $<10\%$ for most levels. Because of the small direct cross section into the $J=0$ $2p_5$ level (see Sec. IV), the cascade contribution to the total apparent cross section for this level may be higher.

The $1s_5 \rightarrow 2p_{10}$ excitation function in Fig. 3 shows a small structure at 1.8 eV, which is 0.5 eV above the excitation threshold. We have examined the $2p_{10}$ excitation function out of the ground level and found a similar structure at the corresponding energy of 0.5 eV above the ground-state excitation threshold. This structure is most likely due to a negative-ion resonance. A similar resonance structure has been reported previously for excitation into the $2p_{10}$ level of Ne [21].

Both metastable targets employed in this work contain a very small fraction of atoms in the $1s_3$ metastable level. For excitation from the $1s_5$ level, the onset energies for excitation into the $2p_{10}$ to $2p_5$ levels range from 1.3–1.6 eV. Since the $1s_3$ level is 1.1 eV higher in energy than the $1s_5$ level, the onset energies for excitation from the $1s_3$ level is 1.1 eV lower (namely, 0.2–0.5 eV). Thus, any signal contribution from excitation of $1s_3$ atoms would be most evident as a nonzero signal in the 0.2–1.3 eV energy range. Excitation from the $1s_3$ metastable level into the $2p_5$–$2p_{10}$ levels are core changing. Experiments on Kr [9] indicate that the energy dependence of a core-changing excitation has a much sharper peak compared to core-preserving excitations. Based on the data of Ref. 9 we estimate that the $1s_3 \rightarrow 2p_n$ $(n>5)$ excitation signal would be most prominent at energies (0.7–1.3 eV) below the onset of excitation from the $1s_5$ level. As seen in Figs. 2–5, the signal at energies below the onset for excitation from the $1s_5$ level is very small. For three of the levels ($2p_5$, $2p_6$, and $2p_{10}$), however, the signal in this energy range is statistically greater than zero. Regardless, this potential $1s_3$ excitation contribution is negligible above the $1s_5$ energy threshold, so our results are solely due to excitation from the $1s_5$ metastable level. This conclusion is consistent with the observation that the $1s_3$ atom number density in our atomic beam is much lower than the $1s_5$ density.

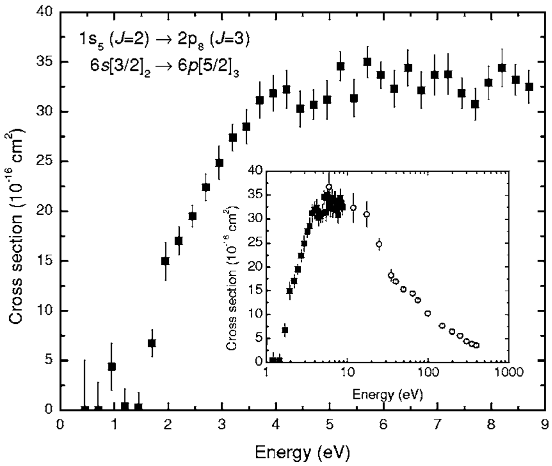

FIG. 5. Excitation function for $J=3$ $2p_8$ level. Error bars are statistical only and do not include the absolute calibration uncertainty of ±35%. The insert includes low-energy data from the hollow cathode source (squares) and high-energy data from the charge exchange source (circles).

We have also attempted to measure fluorescence emissions for excitation into the $2p_1$–$2p_4$ levels. No significant metastable excitation signals were detected. The signal size depends on both the magnitude of the excitation cross section and the target number density. Since the $1s_5$ number density is sufficient to observe signal for excitation into the lower tier levels, the cross sections into the upper tier levels ($2p_1$–$2p_4$) from the $1s_5$ metastable level must be very small (i.e., $\ll 0.2\times 10^{-16}$ cm^2 for the $2p_4$ level). The excitation cross sections into the $2p_1$–$2p_4$ levels from the $1s_3$ metastable level may be large [9]; however, the $1s_3$ number density in the target is too small to produce a significant signal.

Two of the cross sections measured in this work have been previously measured by Mityureva and Smirnov [22].

TABLE III. Apparent cross section values from the $1s_5$ metastable level. Uncertainties in the values are ±35%.

Energy (eV)	Cross section (10^{-16} cm^2)					
	$2p_5$	$2p_6$	$2p_7$	$2p_8$	$2p_9$	$2p_{10}$
2	0.70	9.1	5.7	15	5.8	6.7
3	0.81	13	4.7	25	9.9	11
4	0.47	15	3.2	32	10	13
5	0.35	15	2.9	31	9.1	14
6	0.32	15	2.2	34	8.4	15
7	0.28	15	1.6	34	7.4	15
8	0.28	14	1.4	33	6.4	14
12		14		32		
25		10		25		
50		7.1		15		
75		4.9		13		
100		4.3		10		
150		3.6		7.6		

In their experiment the metastable atoms were created by electron excitation in a Xe gas cell (40–100 mTorr). One high-energy ($\sim$13 eV) pulse was applied to create the metastable atoms, and a second lower-energy pulse was used to excite metastable atoms. The metastable density was measured in an absorption measurement, whereas the optical efficiency was accounted for by ratioing the results to the ground-state cross sections at 13 eV. Their results for the peak $1s_5 \rightarrow 2p_8$ and $1s_5 \rightarrow 2p_6$ cross sections are 240 and 17×10^{-16} cm^2, respectively. In comparison, we obtain 34 and 15×10^{-16} cm^2, respectively, for the two values. The results of the two experiments for excitation into the $2p_6$ level are surprisingly close, considering that the values for the $2p_8$ level differ by a factor of seven.

IV. DISCUSSION

In Secs. IV A and IV B, we explore, qualitatively, how the excitation cross section into a level varies with two key quantum numbers of the final state: the core angular momentum j_c (Sec. IV A) and the total angular momentum J (Sec. IV B). We offer in Sec. IV C a quantitative analysis based on comparing the electron-excitation process to the photon-excitation process through the use of the Born-Bethe approximation. Comparisons are made to the excitation of other metastable atoms and excitation from the ground-state atom (Sec. IV D). Applications of Xe* excitation cross sections are discussed in Sec. IV E. The only theoretical calculation we have located for excitation out of metastable levels was by Hyman based on the Born approximation [23]. The cross sections given therein are averaged over the configuration and, therefore, do not directly correspond to our measurements.

A. Core propensity: Δj_c variation

A general pattern that first emerged in the study of electron-impact excitation out of the metastable levels of Kr is that cross sections for excitations with the same ion core have much larger cross sections than core-changing excitations [9]. This feature was not as apparent in the results of similar experiments for Ar and Ne [16,17]. For the low-lying levels of Ar and Ne, the relatively weak spin-orbit interaction of the ion core (compared to Kr) is decoupled by the Coulomb force of the outer electron so that the core angular momentum is not a good quantum number and no core-related selection rule is readily evident. On the other hand, the Xe$^+$($5p^5$) core has a larger spin-orbit splitting than does Kr$^+$($4p^5$). The core propensity is indeed observed in the Xe cross-section data in that excitation cross sections out of the $1s_5$ ($^2P_{3/2}$ core) into $2p_x$ levels with the same $^2P_{3/2}$ core are large, whereas excitation into $2p_x$ levels with the other ($^2P_{1/2}$) core are very small and generally below the limit of our detection. Because of the exceptionally low abundance of $1s_3$ metastables in our atomic beam target, no measurements were made for excitation from the $1s_3$ level.

B. Multipole field model: ΔJ variation

A simple working model to understand electron excitation in relation to optical excitation has been discussed in our earlier report on Ar [17]. The target atom is subject to a time-dependent electric field with various multipole components produced by the colliding electron. The electric field associated with each multipole component has Fourier components at the frequency necessary to excite the atom into higher-lying levels. Unlike an electromagnetic wave, the electric field due to the colliding electron has a time-dependent longitudinal component and includes a monopole term in addition to the dipole, quadrapole, and higher members. Quantitative application of this model has been made by Purcell to calculate the probability of the $2^2S \rightarrow 2^2P$ transition in hydrogen induced by electron and ion collisions [24].

This model has provided considerable insights to excitation out of the metastable [17] and ground [25,26] levels of argon. For excitation from the Ar $3p^5 4s$ metastable levels the initial level has either $J=2$ ($1s_5$) or $J=0$ ($1s_3$) and the final level is a member of $3p^5 4p$ with $J=0$, 1, 2, or 3. As a one-electron transition, the $4s \rightarrow 4p$ excitation is of the dipole variety. The dipole selection rules allow transitions from $1s_5$ to any level with $J=1,2,3$ of the $3p^5 4p$ configuration, but only the $3p^5 4p$ $J=1$ levels are optically connected to the $1s_3$ metastable level. Experimentally, excitation cross sections corresponding to these two sets of optically allowed processes are found to have "large" cross sections, whereas cross sections for excitation from $1s_3$ into the $J=2$ and $J=3$ levels of $3p^5 4p$ are "small" (i.e., the signals are within the noise level). Excitation into the $J=0$ levels from either $1s_3$ or $1s_5$ is dipole forbidden. The cross sections into these levels indeed are much smaller than those corresponding to dipole-allowed transitions.

The shape of a process's excitation function (i.e., the energy dependence of cross section values) is also related to the multipole component involved in the excitation process. Dipole excitation processes generally have a broad peak that decreases only slowly with increasing electron energy. In contrast, dipole-forbidden processes, which rely on higher-order multipole components (or electron exchange), have sharply peaked excitation functions that decrease rapidly with electron energy. Using excitation of metastable argon as an example, the average $Q(10 \text{ eV})/Q(5 \text{ eV})$ ratio for eight dipole-allowed processes is 0.9, whereas this ratio is 0.4 for excitation into the two levels with $J=0$ that are dipole forbidden from both metastable levels.

Applying this model to excitation from the $J=2$ $1s_5$ metastable level of Xe, excitation is via the dipole component for the $2p_6$ through $2p_{10}$ levels. As seen in Figs. 3–5 these excitation functions generally have relatively broad excitation functions. Excitation into the Xe $J=0$ $2p_5$ level is dipole forbidden from the $J=2$ $1s_5$ metastable level. Indeed, the measured peak cross section into this level is substantially smaller than the dipole-allowed excitations. The energy dependence of the $1s_5 \rightarrow 2p_5$ cross section is also much more sharply peaked (see Fig. 2). In comparison to excitation from the metastable levels of argon, however, the excitation functions for xenon show a wider continuum of shapes for the dipole-allowed processes. For the $2p_6$, $2p_8$, and $2p_{10}$ levels, the excitation function is very flat from 4 to 8 eV. The excitation function for the $2p_9$ level, however, decreases by 40% over this interval, and that of the $2p_7$ level decreases by 55%

TABLE IV. Comparison of excitation cross sections out of the $1s_5$ metastable level at 8 eV. The Born-Bethe values have been scaled to match our experimental $1s_5 \rightarrow 2p_8$ value. See Eq. (5).

			Cross section (10^{-16} cm^2)	
Level	E_{ij} (eV)	f_{ij} [a]	Scaled Q_{ij}^{BB}	This exp. (8 eV)
$2p_1$	2.82		0	small
$2p_2$	2.76	0.0014	0.040	small
$2p_3$	2.74	0.0024	0.068	small
$2p_4$	2.64	0.0006	0.018	small
$2p_5$	1.62		0	0.28
$2p_6$	1.51	0.24	14	14
$2p_7$	1.48	0.013	0.77	1.7
$2p_8$	1.41	0.56	(33)	33
$2p_9$	1.37	0.12	7.1	6.4
$2p_{10}$	1.27	0.24	14	14

[a] Average of length and velocity values from Ref. 19.

even though these are dipole-allowed excitations. These differences can be analyzed using the multipole field model in a more quantitative way by comparing the oscillator strengths of the corresponding optical transitions as described in Sec. IV C.

C. Born-Bethe theory and relations to oscillator strength

The relation between excitation cross sections and oscillator strengths can be expressed more quantitatively through the Born-Bethe approximation. Within this approximation the $i \rightarrow j$ excitation cross section Q_{ij} as a function of electron energy E is

$$Q_{ij}^{BB}(E) \simeq 4\pi a_0^2 f_{ij} \frac{R^2}{E E_{ij}} \ln E, \tag{5}$$

where a_0 is the Bohr radius, R is the Rydberg energy, E_{ij} is the energy difference between the two energy levels, and f_{ij} is the oscillator strength of the $i \rightarrow j$ transition. Since this expression neglects higher-order E^{-n} terms, it is only expected to be valid at high energies. Indeed, this approximation can be used to test the quality of the absolute calibration procedure. In a plot of $Q_{ij}E$ versus $\ln E$, the slope (at high energies) is proportional to the oscillator strength f_{ij}. For the $1s_5 \rightarrow 2p_8$ and $1s_5 \rightarrow 2p_6$ excitation cross sections, for which we have measurements up to 500 eV, the extracted oscillator strengths are 0.59 ± 0.19 and 0.30 ± 0.10, respectively, which compare favorably to theoretical values of 0.56 and 0.24 [19]. Very near threshold the Born cross sections for dipole-allowed transitions are typically too large by a factor of two [27]. Nevertheless, in Table IV we can still illustrate the dependence on the oscillator strength at low electron energies by scaling the Born-Bethe results by a fixed constant to normalize the $1s_5 \rightarrow 2p_8$ cross section to the observed value.

For the four strongest transitions ($1s_5 \rightarrow 2p_6, 1s_5 \rightarrow 2p_8, 1s_5 \rightarrow 2p_9, 1s_5 \rightarrow 2p_{10}$), we see a proportionality relation within 10%. The $1s_5 \rightarrow 2p_7$ oscillator strength is an order of magnitude smaller than the four large ones. This excitation cross section is not entirely due to dipole coupling, and other modes of interaction make the cross section larger than what is expected from dipole consideration alone (as seen in Table IV). The $1s_5 \rightarrow 2p_5$ is dipole forbidden, and the cross section is the smallest of the core-preserving $1s_5 \rightarrow 2p_x$ group.

The continuum of excitation function shapes can also be understood in terms of the magnitudes of the optical oscillator strengths and the Born-Bethe theory. The dipole component (E^{-1} ln E) of the Born-Bethe expansion yields a broad peak in the excitation function for the 0–9 eV range considered here. Higher-order terms ($E^{-2}, E^{-3}, \ldots$) and electron exchange produce a sharper peak located within a few electron volts of the onset energy. The $1s_5 \rightarrow 2p_8$, $1s_5 \rightarrow 2p_6$, $1s_5 \rightarrow 2p_{10}$ excitation functions with the three largest optical oscillator strengths (0.56, 0.24, 0.24) constitute the one class with a broad peak characteristic of dipole-allowed excitation. On the other extreme is the $1s_5 \rightarrow 2p_5$ excitation, which has a zero dipole-coupling component, and thus proceeds only through higher-order processes. Here the excitation function exhibits a very sharp peak that drops off by 60% within 1 eV of the peak. Between these two extremes is $1s_5 \rightarrow 2p_7$, which has a rather small oscillator strength of 0.013. We still observe a fairly sharp peak (see Fig. 3), but with a more gentle decline compared to the $1s_5 \rightarrow 2p_5$ extreme, evidently due to the presence of the small (but nonzero) dipole-type coupling. Finally, we have a different intermediate case $1s_5 \rightarrow 2p_9$ with a medium oscillator strength 0.12. The excitation function does have a slight peak characteristic of the presence of higher-order components, but the excitation function is still fairly broad, like the typical dipole shape.

D. Comparison with ground-state excitation

One objective of a systematic study of electron excitation out of the metastable levels is to understand how it differs from excitation out of the ground level and to identify the underlying principles governing their difference. To this end we examine the ratio of the peak excitation cross section into a given final level f out of a metastable level m to the peak cross section into the same final level out of the ground level g. For the case of Ar, this ratio varies from 15 to 700 for excitation into the $2p_x$ levels. This large variation can be understood from the results of the multipole field model (see Sec. IV B). Excitation from both the $1s_3$ ($J=0$) and $1s_5$ ($J=2$) metastable levels into the $2p_1$ ($J=0$) and $2p_5$ ($J=0$) levels have relatively small cross sections compared to the other $2p_x$ levels because these particular excitations are forbidden by the dipole selection rule $\Delta J = 0, \pm 1, 0 \not\rightarrow 0$. For excitation out of the ground level, however, the $2p_1$ and $2p_5$ levels have relatively large cross sections because the multipole analysis generally favors excitation from the ground level into even-J levels over odd-J levels for the $2p_x$ series [25,26]. This combination places the ratio $Q(m \rightarrow f)/Q(g \rightarrow f)$ at the lower edge of its range, equal to 15 and 27 for $f = \mathrm{Ar}(2p_1)$ and $\mathrm{Ar}(2p_5)$ respectively [17]. For the $\mathrm{Ar}(2p_9)$ this ratio becomes 500 because the $1s_5 \rightarrow 2p_9$ excitation satisfies the dipole selection rule and has one of the largest cross sections.

The cross section data on Kr and Xe allow similar comparison of excitation out of the ground level and metastable levels. For instance, the $Q(m \rightarrow f)/Q(g \rightarrow f)$ ratio is 6.5 and 520, respectively, for $\mathrm{Kr}(2p_5)$ and $\mathrm{Kr}(2p_9)$ [9]. The corresponding ratios for the lower $J=0$ level and the $J=3$ level of the $\mathrm{Xe}(5p^5 6p)$ configuration are 8.3 and 200, respectively. (Note that in Xe, the $J=3$ level is labeled as the $2p_8$ rather than the $2p_9$ as is the case for the other rare gases.) The general feature of the wide range of ratios for different $2p_x$ levels is preserved, but with a slightly reduced range. This narrowing of the range of values is due, in part, to the fact that the cross sections for excitation out of the ground state increase more rapidly as one moves along the Ne$\rightarrow$Xe progression than do the cross sections out of the metastable levels. The peak direct cross section for excitation into the $J=3$ level from the ground state increases by over a factor of 20 in moving from Ne (ionization energy 21.6 eV) to Xe (12.1 eV). In contrast, the peak cross section for excitation into the $J=3$ level from the $1s_5$ metastable level increases by only about factor of two in moving from Ne* (4.9 eV) to Xe* (3.8 eV).

E. Applications

The wide variation of the $Q(m \rightarrow f)/Q(g \rightarrow f)$ ratio over the $2p$ series has provided the basis for different techniques in optical plasma diagnostics. In a low-temperature plasma containing a small fraction of metastable atoms, a given level f in the $2p$ series can be populated by an inelastic collision of a ground-state atom with a "high" energy electron or an inelastic collision with a metastable atom and a "low" energy electron. For sufficiently large metastable number densities, some levels, such as $\mathrm{Ar}(2p_9)$, are populated mostly through the second route, while other levels, such as the $\mathrm{Ar}(2p_1)$, are mostly populated by ground-state excitation. Thus, measurements of emission intensities from the various $\mathrm{Ar}(2p)$ levels provide an effective means to study the electron energy distribution function and also the metastable atom density [28,29]. Knowledge of the $Q(m \rightarrow f)/Q(g \rightarrow f)$ ratio for different $2p$ levels of all the rare-gas atoms is important for increasing the number of energy regions probed in those types of plasma diagnostics that use mixtures of rare-gas atoms, such as TRG-OES [7].

ACKNOWLEDGMENTS

The authors wish to thank B. Chiaro for his assistance with the discharge lamp calibration. Support by the National Science Foundation is gratefully acknowledged.

[1] S. Gortchakov, H. Lange, and D. Uhrlandt, J. Appl. Phys. **93**, 9508 (2003).
[2] T. Shiga, L. C. Pitchford, J.-P. Boeuf, and S. Mikoshiba, J. Phys. D **36**, 512 (2003).
[3] T. J. Sommerer, J. Phys. D **29**, 769 (1996).
[4] Y. B. Golubovskii, I. A. Porokhova, H. Lange, S. Gortchakov, and D. Uhrlandt, Plasma Sources Sci. Technol. **14**, 45 (2005).
[5] D. Hayashi, G. Heusler, G. Hagelaar, and G. Kroesen, J. Appl. Phys. **95**, 1656 (2004).
[6] J. B. Boffard, C. C. Lin, and C. A. DeJoseph, J. Phys. D **37**, R143 (2004).
[7] V. M. Donnelly, J. Phys. D **37**, R217 (2004).
[8] M. V. Malyshev and V. M. Donnelly, Phys. Rev. E **60**, 6016 (1999).
[9] R. O. Jung, T. E. Stone, J. B. Boffard, L. W. Anderson, and C. C. Lin, Phys. Rev. Lett. **94**, 163202 (2005).
[10] R. B. Lockwood, L. W. Anderson, and C. C. Lin, Z. Phys. D: At., Mol. Clusters **24**, 155 (1992).
[11] J. B. Boffard, M. E. Lagus, L. W. Anderson, and C. C. Lin, Rev. Sci. Instrum. **67**, 2738 (1996).
[12] A. R. Filippelli, C. C. Lin, L. W. Anderson, and J. W. McConkey, Adv. At., Mol., Opt. Phys. **33**, 1 (1994).
[13] M. E. Lagus, J. B. Boffard, L. W. Anderson, and C. C. Lin, Phys. Rev. A **53**, 1505 (1996).
[14] G. E. Ice and R. E. Olson, Phys. Rev. A **11**, 111 (1975).
[15] J. T. Fons and C. C. Lin, Phys. Rev. A **58**, 4603 (1998).
[16] J. B. Boffard, M. L. Keeler, G. A. Piech, L. W. Anderson, and C. C. Lin, Phys. Rev. A **64**, 032708 (2001).
[17] J. B. Boffard, G. A. Piech, M. F. Gehrke, L. W. Anderson, and C. C. Lin, Phys. Rev. A **59**, 2749 (1999).
[18] H. Horiguchi, R. S. F. Chang, and D. W. Setser, J. Chem. Phys. **75**, 1207 (1981).
[19] M. Aymar and M. Coulombe, At. Data Nucl. Data Tables **21**, 537 (1978).
[20] J. B. Boffard, M. F. Gehrke, M. E. Lagus, L. W. Anderson, and C. C. Lin, Eur. Phys. J. D **8**, 193 (2000).
[21] F. A. Sharpton, R. M. St. John, C. C. Lin, and F. E. Fajen, Phys. Rev. A **2**, 1305 (1970).
[22] A. A. Mityureva and V. V. Smirnov, Opt. Spektrosk. **74**, 12 (1993), [Opt. Spectrosc. **74**, 6 (1993)].
[23] H. A. Hyman, Phys. Rev. A **24**, 1094 (1981).
[24] E. M. Purcell, Astrophys. J. **116**, 457 (1952).
[25] J. E. Chilton, J. B. Boffard, R. S. Schappe, and C. C. Lin, Phys. Rev. A **57**, 267 (1998).
[26] J. E. Chilton and C. C. Lin, Phys. Rev. A **60**, 3712 (1999).
[27] Y.-K. Kim, Phys. Rev. A **64**, 032713 (2001).
[28] S. A. Moshkalyov, P. G. Steen, S. Gomez, and W. G. Graham, Appl. Phys. Lett. **75**, 328 (1999).
[29] Y. Miyoshi, Z. L. Petrovic, and T. Makabe, J. Phys. D **35**, 454 (2002).